ARL-MR-1154 ● MAY 2026

Molecular Beam Epitaxially Grown Catalysts for FY25 Blue Carbon–Direct Air Capture Program

by David R. Baker, Vijay S. Parameshwaran, and Caroline M. Hill

NOTICES

Disclaimers

The findings in this report are not to be construed as an official Department of the Army position unless so designated by other authorized documents.

Citation of manufacturer's or trade names does not constitute an official endorsement or approval of the use thereof.

Destroy this report when it is no longer needed. Do not return it to the originator.

ARL-MR-1154 ● MAY 2026

Molecular Beam Epitaxially Grown Catalysts for FY25 Blue Carbon–Direct Air Capture Program

David R. Baker and Vijay S. Parameshwaran
DEVCOM Army Research Laboratory

Caroline M. Hill
General Technical Services

REPORT DOCUMENTATION PAGE

1. REPORT DATE	2. REPORT TYPE	3. DATES COVERED	
		START DATE	END DATE
May 2026	Memorandum Report	1 October 2024	30 September 2025

4. TITLE AND SUBTITLE
Molecular Beam Epitaxially Grown Catalysts for FY25 Blue Carbon–Direct Air Capture Program

5a. CONTRACT NUMBER	5b. GRANT NUMBER	5c. PROGRAM ELEMENT NUMBER
5d. PROJECT NUMBER	**5e. TASK NUMBER**	**5f. WORK UNIT NUMBER**

6. AUTHOR(S)
David R. Baker, Vijay S. Parameshwaran, and Caroline M. Hill

7. PERFORMING ORGANIZATION NAME(S) AND ADDRESS(ES)	8. PERFORMING ORGANIZATION REPORT NUMBER
DEVCOM Army Research Laboratory ATTN: FCDD- RLA-GC Adelphi, MD 20783-1138	ARL-MR-1154

9. SPONSORING/MONITORING AGENCY NAME(S) AND ADDRESS(ES)	10. SPONSOR/MONITOR'S ACRONYM(S)	11. SPONSOR/MONITOR'S REPORT NUMBER(S)
Office of Naval Research Code 32 Arlington, VA 22203-1995		

12. DISTRIBUTION/AVAILABILITY STATEMENT
DISTRIBUTION STATEMENT A. Approved for public release: distribution unlimited.

13. SUPPLEMENTARY NOTES
ORCID(s): David R. Baker, 0000-0002-9930-5183; Vijay S. Parameshwaran, 0009-0004-0288-9170; Caroline M. Hill, 0000-0001-8196-9769

14. ABSTRACT
The selectivity of products from the carbon dioxide reduction reaction (CO2RR) is highly diverse because of similar reaction potentials for a variety of products. Crystal facets of electrocatalysts have had implied impact on CO2RR selectivity but definitive causation is hampered by the heterogeneous surface states inherent to nanoparticle geometries. Molecular beam epitaxy (MBE) allows for copper (Cu) electrocatalyst growth to be controlled in a single-crystal format. This effort explores multiple crystal orientations of Cu and Cu alloys grown as single-crystal films with MBE and monitoring the reaction products. Substrates are single-crystal silicon wafers to aid in controlling the growth direction and were sent to a partner for CO2RR product analysis in an H-cell configuration. Additionally, the same deposition recipes are used to grow on fibrous gas diffusion electrodes and are tested in a zero-gap cell to explore initial scale-up effects, specifically tracking the production of ethylene.

15. SUBJECT TERMS
Energy Sciences, carbon dioxide, ethylene, molecular beam epitaxy, electrochemistry, alternative fuels

16. SECURITY CLASSIFICATION OF:			17. LIMITATION OF ABSTRACT	18. NUMBER OF PAGES
a. REPORT	b. ABSTRACT	C. THIS PAGE		
UNCLASSIFIED	UNCLASSIFIED	UNCLASSIFIED	UU	21

19a. NAME OF RESPONSIBLE PERSON	19b. PHONE NUMBER *(Include area code)*
David R. Baker	(520) 691-6416

STANDARD FORM 298 (REV. 5/2020)
Prescribed by ANSI Std. Z39.18

Contents

List of Figures

List of Tables

1. Introduction

Carbon dioxide (CO_2) reduction to fuels is an attractive process to generate fuels at the point of need due to the lower temperatures and balance of plants needed for chemical conversion compared to the traditional Fischer–Tropsch process. The selectivity of the CO_2 reduction reaction (CO2RR) for a specific fuel is critical to its application because it defines several efficiency metrics and has implications for back-end separations of CO2RR products. Typically, an electrochemical reaction's selectivity can be tailored using specific potentials of reaction, but CO2RR has many potential reactions within a narrow electrochemical window and the hydrogen evolution reaction is also a persistent deleterious participant (Equations 1–5).

$$CO_2 + 2H^+ + 2e^- \rightarrow CO(g) + H_2O \qquad (E^0 = -0.1\ V) \qquad (1)$$

$$CO_2 + 2H^+ + 2e^- \rightarrow HCOOH(eq) \qquad (E^0 = -0.12\ V) \qquad (2)$$

$$2H^+ + 2e^- \rightarrow H_2 \qquad (E^0 = 0\ V) \qquad (3)$$

$$CO_2 + 8H^+ + 8e^- \rightarrow CH_4(g) + 2H_2O \qquad (E^0 = 0.17\ V) \qquad (4)$$

$$2CO_2 + 12H^+ + 12e^- \rightarrow C_2H_4(g) + 4H_2O \qquad (E^0 = 0.08\ V) \qquad (5)$$

For the CO2RR, copper (Cu) is a common catalyst that has demonstrated good faradaic efficiencies for CO_2 reduction to C2 species including ethylene. The selectivity of Cu is thought to be a function of the crystal facet index on which the CO_2 is reduced, and previous research has shown changes in faradaic efficiencies for Cu(111), Cu(751), and Cu(100) thin films.[1]

To expand on our previous research in this program, in FY25 the U.S. Army Combat Capabilities Development Command (DEVCOM) Army Research Laboratory (ARL) investigated the fabrication of Cu single-crystal surfaces as well as expanding the single-crystal search to include crystal facets of Cu bimetallic alloys including aluminum (Al), gallium (Ga), and indium (In), which have shown high CO2RR activity in our recent work.[2] During that time, ARL was able to produce molecular beam epitaxy (MBE) substrates on gas diffusion layer (GDL) electrodes made of Cu and Cu alloys. These were used to develop the growth rates of the materials and to allow integration into the alkaline reactor. The GDL geometry did not allow for single-crystal investigation (due to the nature of the polycrystalline carbon paper substrates) but did show high faradaic efficiency toward C2 products and carbon monoxide (CO) depending on the reactor conditions.

For the FY25 effort, the MBE-grown Cu and Cu-alloy films were both grown as 1) single-crystal electrodes to be tested for fundamental activity and selectivity analysis and 2) electrodes on GDL with matching growth parameters as the single-crystal study to identify reactor geometry impacts on performance. ARL's previous effort was able to use electrode engineering techniques to successfully minimize the HER.[2] This year's effort looked more fundamentally at the catalyst alone to improve CO2RR selectivity which had the effect of reintroducing large HER as a side product, but the study was able to specifically target the impact of the Cu-based catalyst formulation on C1 versus C2 selectivity.

2. Approach

2.1 Single-Crystal Cu and Cu Alloys

To aid ARL in the electrochemical analysis of the CO2RR, the Mirkin lab at Northwestern University (NU) was provided single-crystal Cu and Cu/Al MBE samples fabricated by ARL. Utilizing their state-of-the-art facilities and capabilities, NU evaluated catalysts via electrochemical setups to determine the CO2RR activity and product selectivity via gas chromatography and nuclear magnetic resonance spectroscopy.

Additionally, megalibraries at NU, containing thousands to millions of catalyst materials in a single centimeter-scale chip, were available to further investigate how different element composition and nanoscale interfacing affect product selectivity. High-throughput screening was targeted via scanning droplet cell measurements in either a four-electrode configuration or in an integrated configuration with in-line product detection, which allowed for the evaluation of selectivity of the electrocatalysts as well as screening for desired product formation. The impact of this work will accelerate the discovery of CO2RR catalysts with enhanced selectivity; thousands of catalysts can be simultaneously compared to evaluate the interplay of composition and structure in catalytic outcome through the megalibrary platform.

2.2 Corresponding Catalysts in Membrane Electrode Assemblies

In addition to the fundamental research performed at NU, the ARL team expanded experimentation to include membrane electrode assemblies (MEAs) of the same material set investigated by NU. Cu and Cu alloys were deposited onto electrodes using the exact MBE conditions, but the electrodes were GDLs made of carbon fibers. This substrate prohibits single-crystal fabrication on the cylindrical fibers. The intention of the MEA work was to show the impact of initial scale-up from

fundamental catalyst analysis, as well as a comparison with the NU studies as an assessment of practical integration of catalysts into MEA-based reactors. ARL investigated product selectivity, current density, and energy efficiency just as in the NU work.

3. Results

3.1 Single-Crystal Electrodes

The MBE growth of the samples sent to NU was of single-crystal epitaxial Cu and CuAl alloys on (111)-oriented silicon, which have been earlier grown and characterized in previous quarterly reports. To give NU a high degree of freedom for testing samples under various conditions to assess CO2RR performance, the samples were grown on 3-inch-diameter wafers such that they could be diced into smaller pieces for a variety of tests. To protect the Cu and CuAl surfaces during shipping, photoresist was spun and baked on the sample. All processing (both materials growth and photoresist coating) were done at temperatures at or below 50 °C to prevent Cu diffusion into silicon. Four wafers were grown and sent: a thick (1.8-µm) Cu layer, a thin (300-nm) Cu layer, a thick (1.8-µm) CuAl layer, and a thin (300-nm) CuAl layer. The nature of all four layers, including alloying, crystallinity, and epitaxial relationship to the silicon substrate, has been characterized in previous reports for this program. As an in-situ method to confirm crystal growth, reflection high-energy electron diffraction (RHEED) images of all four materials were captured, showing a single-crystal nature without any degradation into polycrystalline material or copper diffusion into silicon to form an amorphous surface. Additionally, prominent Kikuchi lines are visible in the RHEED pattern, demonstrating the good long-range order and crystalline quality of the Cu and CuAl electrocatalyst samples.[3] These images are shown in Figure 1. The quantitative product analysis at NU is ongoing at the time of this report.

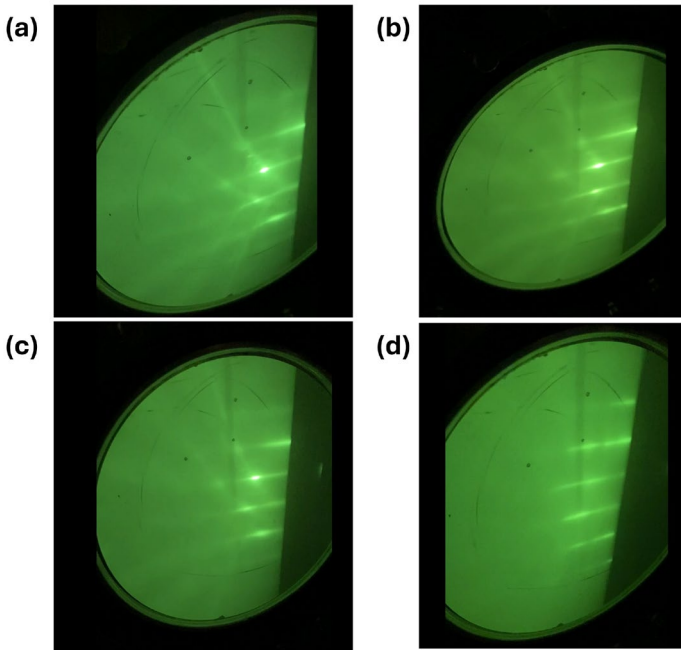

Figure 1. RHEED patterns of (a) thick Cu, (b) thin Cu, (c) thick CuAl, and (d) thin CuAl grown by MBE on 3-inch (111)-oriented silicon substrates.

3.2 Membrane Electrode Assemblies

3.2.1 Characterization

MBE growths of Cu and Cu alloys (CuAl with three different Al concentrations, CuGa, and CuIn) on polycrystalline carbon paper substrates were fabricated for testing at ARL. For this study, the number after a CuAl alloy label was the target Al percent in the alloy—e.g., the amount of Al is 10% the amount of Cu in "CuAl 10." Surface composition of each sample prior to experimentation was characterized by X-ray photoelectron spectroscopy (XPS) and X-ray diffraction (XRD).

Table 1 shows the beam-equivalent pressure (BEP) representing the fluxes of the constituent elements for the growth of all alloy samples. In all growth experiments, the Cu cell temperature was kept constant (1150 °C base, 1350 °C tip), hence the variability of the fluxes across different samples. The flux of the Group III metals was adjusted corresponding to the targeted percentage of the Cu flux; e.g., the Al/Cu flux ratio of CuAl 10 is 2.24E-8/2.22E-7 = 10%. The substrate temperature of all growths was 200 °C.

Table 1. MBE sample and BEPs measured before copper/alloy film deposition.

MBE sample	Cu BEP flux (Torr)	Al BEP flux (Torr)	Ga BEP flux (Torr)	In BEP flux (Torr)
Cu	2.28E-7	0	0	0
CuAl 10	2.22E-7	2.24E-8	0	0
CuAl 30	1.94E-7	5.80E-8	0	0
CuAl 50	2.19E-7	9.98E-8	0	0
CuGa	2.40E-7	0	2.61E-8	0
CuIn	2.33E-7	0	0	2.35E-8

XPS survey scans for all six samples are shown in Figure 2. Binding energies for Cu, carbon (C), and oxygen (O) appear where expected for all materials. In3d peaks are present for CuIn in the appropriate 445- to 455-eV range. Peaks for Ga are less evident in the CuGa sample but are present at the 3d (20 eV), 3p (105 eV), and LMM Auger (423 eV) locations. The binding energies of Al are known for overlapping with Cu and are difficult to separate, thus close-up scans of the Al 2s and Cu 3s peaks are shown in Figure 3 for the Cu only and Cu/Al alloyed samples. This figure shows the qualitative increase in Al at the 2s peak location (119 eV, right) from zero Al alloying (Cu) to the highest Al alloying (CuAl 50). Quantitative ratios of alloys in all six samples, determined by extracting peak intensities for each element, are summarized in Table 2.

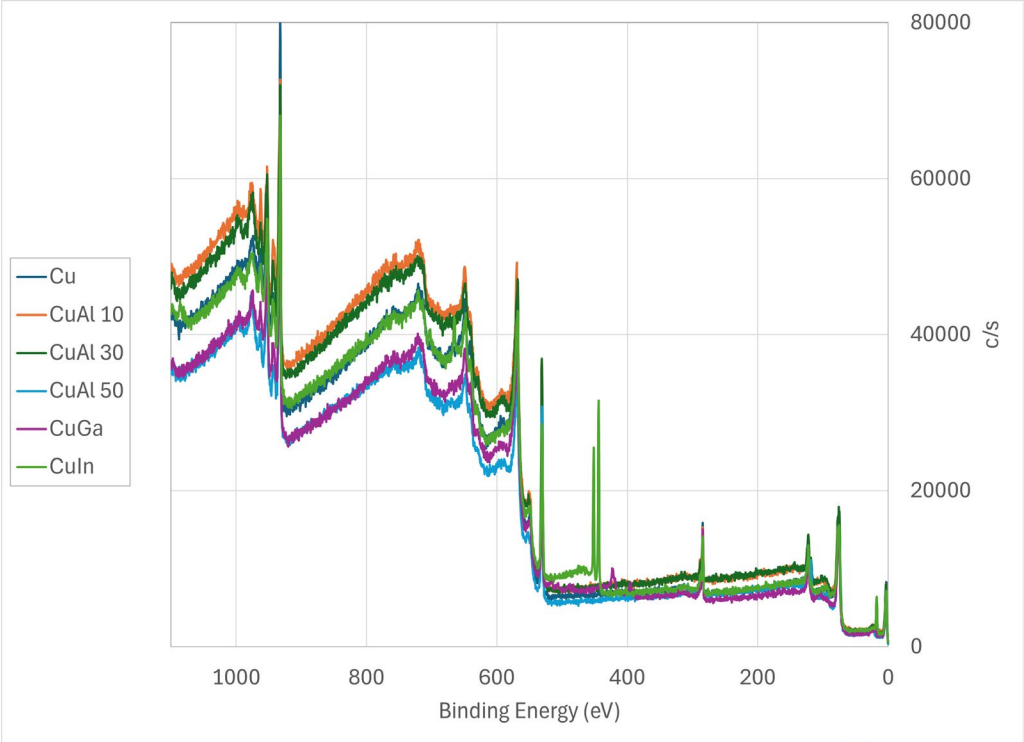

Figure 2. Survey XPS scans from 0 to 1100 eV for six samples of Cu or Cu alloys on carbon paper: Cu only, three alloys of Cu and Al (Caulk 10, CuAl 30, and CuAl 50), CuGa, and CuIn.

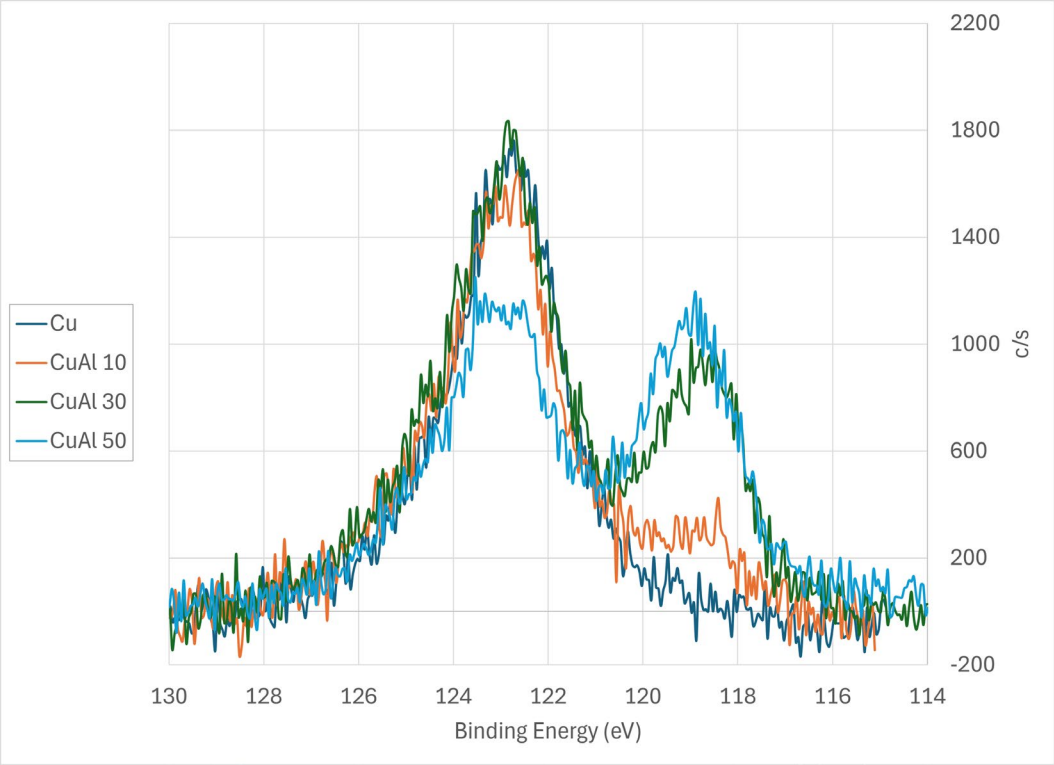

Figure 3. Background subtracted XPS scans at the location of the Al 2s peak (119 eV, right) and Cu 3s peak (123 eV, left) for Cu only and Cu/Al alloyed samples on carbon paper.

Table 2. Ratios of alloying metals in the surface composition of each sample determined using XPS.

MBE sample	Alloying metal ratio
Cu	100% Cu
CuAl 10	10% Al, 90% Cu
CuAl 30	28% Al, 72% Cu
CuAl 50	44% Al, 56% Cu
CuGa	15% Ga, 85% Cu
CuIn	17% In, 83% Cu

XRD scans of all samples are shown in Figure 4. Due to the thin layer of approximately 300 nm and the polycrystallinity of the materials from growing on a carbon paper substrate, the signal intensity is not high, but important insights are obtained as to the nature of these films. Most films, except for CuAl 50, are predominantly in the face-centered cubic (FCC) copper phase, with shifts in the Cu (111) diffraction peak (nominally at a 2θ angle of 43.317°) reflecting a shift in the lattice constant due to the dilute alloying of the constituent Group III metal. This effect is more obvious in thicker 1.7-µm variants of Cu, CuAl 10, CuIn, and CuGa grown on carbon paper as shown in Figure 5. By incorporating more Al in CuAl 30, the diffraction peak shifts more markedly to a lower angle as a reflection of the

additional alloying within the Cu phase, but from incorporating even more Al in CuAl 50, the peak shifts to a higher angle of 44.18°. This implies a potential phase change and/or separation from FCC Cu across an intermetallic Cu_4Al and Cu_9Al_4 (which has a dominant (330) diffraction peak at 44.091° from the powder diffraction file, Ref. no. 98-000-1625).

In addition to the chemical and elemental alloying determined by XPS, determination of the specific crystal phase carries implications for ethylene Faradaic efficiency and selectivity. Additional MBE growth experiments, specifically thicker films across a broader range of Cu-Al flux ratios, and on single-crystal substrates, are required to perform thorough XRD analysis that gets at the nature of low-Al CuAl crystallographic alloying and phase transformations/ separations as shown in the binary phase diagram in Figure 6.

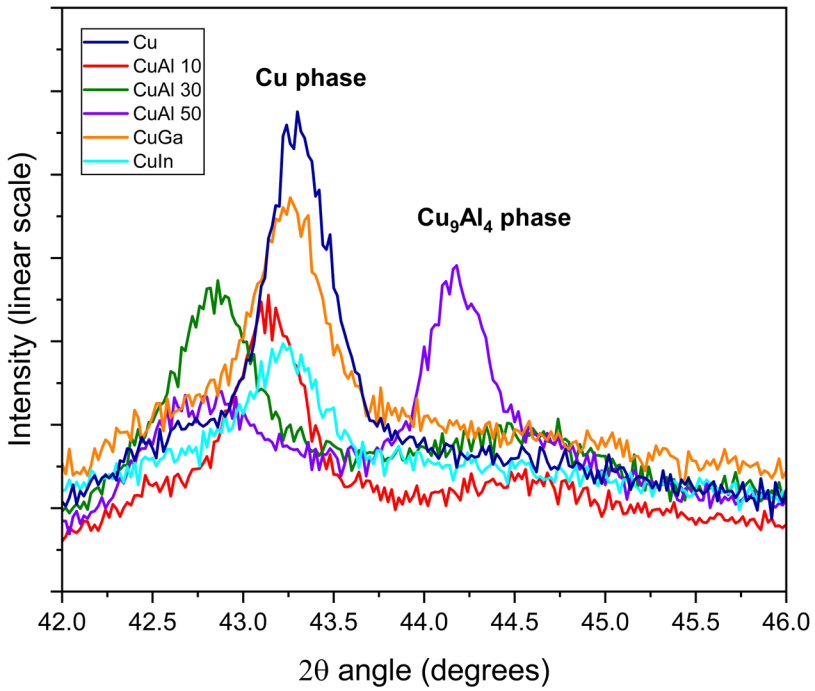

Figure 4. Symmetric 2θ-ω XRD scans for six samples of Cu or Cu alloys on carbon paper: Cu only, three alloys of Cu and Al (CuAl 10, CuAl 30, and CuAl 50), CuGa, and CuIn.

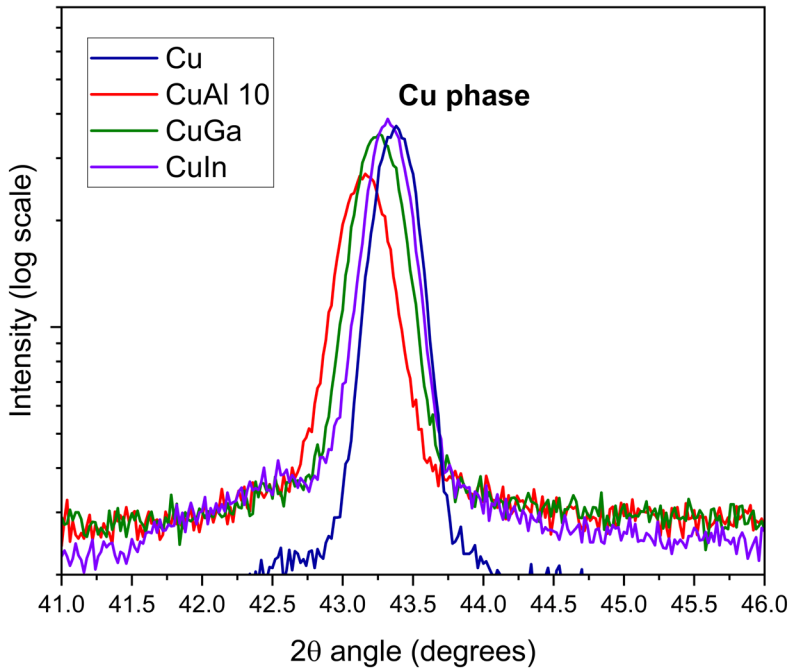

Figure 5. Symmetric 2θ-ω XRD scans for four thick (1.7-μm) samples of Cu or Cu alloys on carbon paper: Cu only, CuAl 10, CuGa, and CuIn.

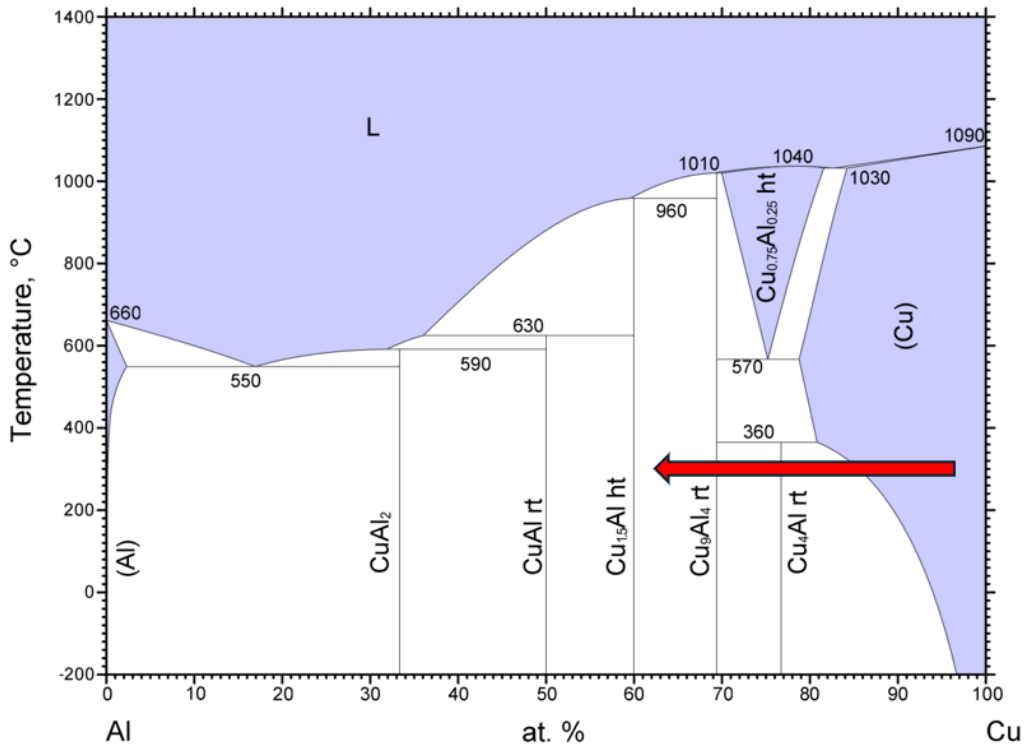

Figure 6. Aluminum-copper binary phase diagram (ASM International, Diagram no. 904228); the red arrow shows the trend of phase transformation and/or separation as the flux ratio is increased from CuAl 10, to CuAl 30, to CuAl 50.

3.2.2 Membrane Electrode Assembly Testing

Samples were electrochemically evaluated in a custom 6.45-cm^2 (1-in^2) MEA test setup. To fabricate each MEA, GDLs were cut to size and the surface, with Cu or Cu-alloy MBE growth, was subsequently coated with 20 mg PTFE. Carbon paper coated with 20 mg of iridium black powder and 100 mg of 5% Nafion solution was used for the anode. The MEA was pressed together between graphite plates, which served as both flow channels and charge conductors. Assembly occurred in the following order: graphite plate, Cu or Cu-alloy GDL (Cu surface facing membrane), Teflon gasket, PiperION anion exchange membrane, Teflon gasket, iridium GDL (iridium surface facing membrane), graphite plate.[2] During all experiments, 0.1 M potassium hydroxide was pumped through the anode side, and 50 mL/min of humid CO_2 was delivered to the cathode side of the cell. Applied potential and measured current density were monitored by an Arbin cell tester. The system was validated with a sample of electrodeposited Cu on GDL before testing the MBE growth GDLs. Electrodeposition of Cu resulted in a faradaic efficiency for ethylene production of 5.9%. Faradaic efficiency was calculated using the following equation, where x is the fraction of gas product obtained from an SRI gas chromatograph (GC), V is the product flow rate, P is the pressure, n is the number of electrons transferred in the reaction, F is Faraday's constant, j is the measured current, R is the gas constant, and T is the cell temperature.

$$F_{\text{eff}} = \frac{xVPnF}{jRT} \times 100\% \tag{6}$$

Exemplary experimental results for the CuAl 30 GDL are shown in Figure 7. Applied potential varied between 3.0 and 3.4 V. Measured current density increased with applied potential and, following a period of fluctuation after each step change in potential, reached a stable value. Gas composition, measured every 30 min, also increased with applied potential. Hydrogen dominated the gas composition at all voltages with only small quantities of carbon dioxide and ethylene present. Other gas species, including methane, acetylene, propylene, and propane, were also measured, but quantities were not significant and thus are not included in the results. Faradaic efficiencies for each gas species did not show the same direct relationship to applied potential as current and gas composition. Hydrogen was relatively stable around 70% with a slight increase to 75% when stepping up to 3.4 V. Hydrogen is a significant portion of the product gas composition but this study was interested in the CO2RR selectivity. Previous years efforts have investigated reactor design methods to reduce the HER relative to CO2RR. CO production showed the opposite trend with a step down from 11% to 5% at 3.4 V. Ethylene faradaic efficiency increased from approximately 5% to 17% when stepping up to 3.2 V and stayed constant at 3.4 V. The faradaic efficiency of ethylene was also high compared to its relatively low

concentration in the product gas composition because of the high number of electrons transferred during the electrochemical reaction (12 for ethylene vs. 2 for hydrogen and carbon monoxide). These results highlight the importance of investigating the effect of variables such as applied potential and current density on product formation rates and energy efficiency.

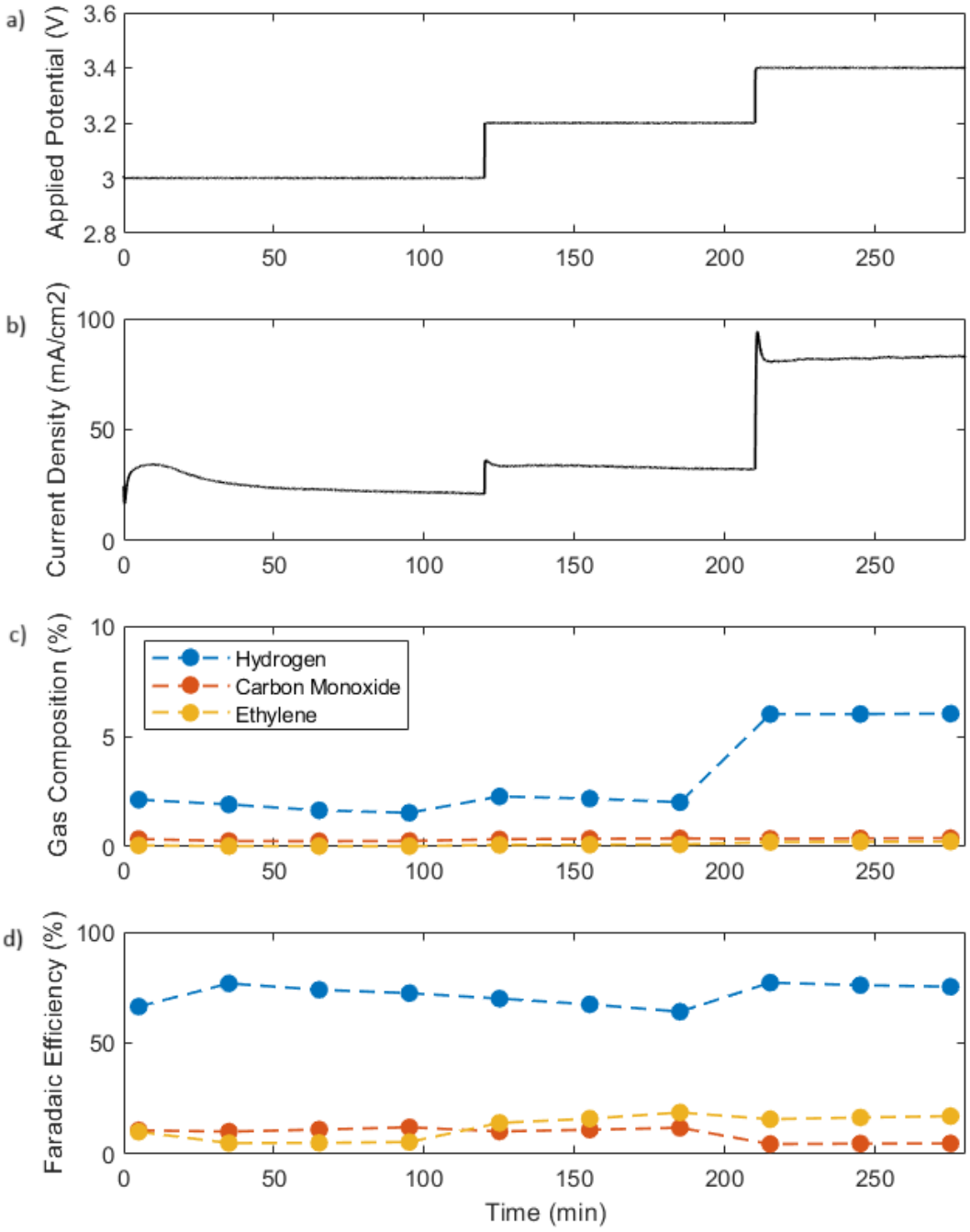

Figure 7. Experiment summary for the CuAl 30 GDL sample: a) potential applied over the course of the experiment, b) measured current density, c) product gas composition measured by the SRI GC, and d) calculated faradaic efficiency for each gas species.

Average current densities and ethylene faradaic efficiencies for all GDL samples at applied potentials from 3.0 to 3.4 V are summarized in Figure 8. Current densities for the CuIn GDL were significantly higher than all other GDL samples and were also unstable, increasing steadily over time. Because of this, experiments with CuIn were discontinued after 3.2 V and no data was collected at 3.4 V. Current densities for all other GDL samples (Cu, CuAl, and CuGa) were stable and followed the same general trend of increasing with applied potential. Cu with no added alloy had the lowest current across the board, and CuAl 10 showed the highest current density at 3.2 and 3.4 V, excluding CuIn.

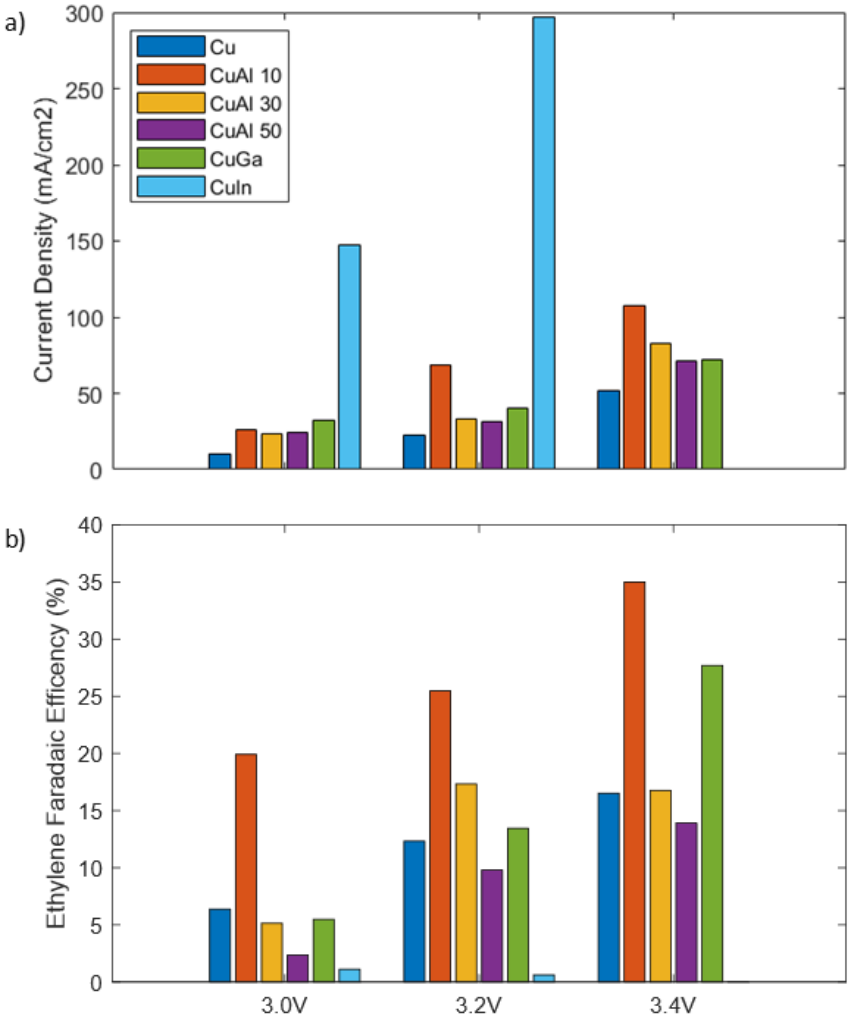

Figure 8. a) Average measured current density and b) ethylene faradaic efficiency at three applied potentials for all Cu and Cu-alloy GDL samples: Cu, CuAl 10, CuAl 30, CuAl 50, CuGa, and CuIn.

At all applied potentials, the CuAl 10 GDL demonstrated the highest ethylene faradaic efficiencies with approximately double the efficiency of the Cu-only GDL. This observation led to testing of different Cu-to-Al ratios; however, ethylene faradaic efficiency decreased with increasing Al content (CuAl 30 and CuAl 50) at all applied potentials. These results indicate that alloying Cu with small quantities of Al can be highly beneficial for ethylene production, but the ratio still needs to be fine-tuned, keeping in mind that the Cu/Al ratio impacts phase transformations and separations, likely also impacting electrocatalytic performance with crystallinity considerations not simply through elemental ratios. The ratio of Al in the CuAl 10 sample was significantly lower than the CuAl 30 sample, 13% versus 48%, respectively, leaving much room for exploration. CuGa performed better than CuAl 30 and CuAl 50 at 3.0 and 3.4 V, but faradaic efficiencies were still lower than the original CuAl 10 sample. Minimal ethylene was produced by the CuIn sample. Combined with significantly higher current densities, ethylene faradaic efficiency for CuIn was close to zero.

4. Conclusions and Future Opportunities

Overall, the best energy efficiencies and current densities were achieved with the CuAl 10 GDL, which demonstrated a two-fold increase in ethylene faradaic efficiency over Cu alone. As Al content increased, performance decreased, indicating the ratio of Cu to Al is critical and requires further investigation. CuGa was stable and had similar or better performance to the Cu-only GDL, so there could be promise in additional studies with this material. In contrast, CuIn GDL was both unstable and had poor selectivity to ethylene. This study also highlights the importance of investigating materials in MEA systems under a variety of conditions (applied potential, current density, flow rate, surface area, membrane material, electrolyte composition, reaction temperature, MEA assembly process) since performance changed significantly with the few variables changed in this study. Comparisons between the MEA reactor geometry and the H-cell design for single crystal studies are still ongoing and will be reported after a full analysis is available.

5. References

1. Hahn C et al. Engineering Cu surfaces for the electrocatalytic conversion of CO2: controlling selectivity toward oxygenates and hydrocarbons. PNAS. 2017;114(23):5918–5923.

2. Baker D, Parameshwaran V, Boltersdorf J, Jiang R. Highly efficient CO_2 conversion to energy-dense fuels with hybrid electrochemical membrane electrode assembly (MEA) technologies. DEVCOM Army Research Laboratory (US); 2025 Jan. Report No.: ARL-TR-10050.

3. Ingle NJC et al. The structural analysis possibilities of reflection high energy electron diffraction. J Phys D Appl Phys. 2010;43:133001.

List of Symbols, Abbreviations, and Acronyms

Al	Aluminum
ARL	Army Research Laboratory
BEP	Beam-Equivalent Pressure
C	Carbon
CO	Carbon Monoxide
CO_2	Carbon Dioxide
CO2RR	Carbon Dioxide Reduction Reaction
Cu	Copper
DEVCOM	U.S. Army Combat Capabilities Development Command
FCC	Face-Centered Cubic
GC	Gas Chromatograph
GDL	Gas Diffusion Layer
MBE	Molecular Beam Epitaxy
MEA	Membrane Electrode Assembly
NU	Northwestern University
O	Oxygen
RHEED	Reflection High-Energy Electron Diffraction
XPS	X-ray Photoelectron Spectroscopy
XRD	X-ray Diffraction

1 (PDF)	DEFENSE TECHNICAL INFORMATION CTR DTIC OCA
1 (PDF)	DEVCOM ARL FCDD RLB CB TECH LIB